

Modeling of Skin Tissue Ablation by Nanosecond Pulses From Ultraviolet to Near-Infrared and Comparison With Experimental Results

Qiyin Fang and Xin-Hua Hu

Abstract—Comprehension of biological tissue ablation by short laser pulses in a broad optical spectrum is of fundamental importance to the understanding of laser-tissue interaction and advancing surgical applications of lasers. We report a new plasma ablation model in which the chromophore ionization pathway is incorporated to explain the skin tissue ablation by nanosecond laser pulses from ultraviolet to near-infrared. A rate equation is solved to examine the effects of chromophore, cascade, and multiphoton ionization on the optical breakdown of the tissue. The wavelength and spot size dependence of the breakdown thresholds have been measured and agreements have been found between the calculated and measured results.

Index Terms—Biological tissues, biomedical applications of optical radiation, laser ablation, optical breakdown, neodymium: YAG lasers.

I. INTRODUCTION

LASER surgery is often accomplished with nanosecond pulses to achieve precise ablation with reduced collateral tissue damage. Ablation of tissues or pigments by a laser pulse is a result of optical breakdown and prominent examples of ablation-based surgical operations include the corneal surgery with the deep ultraviolet (UV) pulses and skin surgery with the visible and near-infrared (NIR) pulses. The breakdown of tissues or pigments by nanosecond laser pulses has attracted active attention, and several models have emerged but none is capable of explaining all major experimental results over a broad spectrum from deep UV to NIR in terms of the underlying breakdown mechanism. A selective photothermolysis model [1] has been proposed that considers the transient heating as the cause of ablation by laser pulses in the visible and NIR regions. It can be used as a guide to estimate the relation between collateral tissue damage and laser parameters, becoming a widely used model of skin tissue ablation for laser pulses of both short and long durations [2]. The underlying assumption of the model, however, is that the ablation is a result of rapid vaporization in tissue due to the absorption of a laser pulse by tissue or pigment and no ionization is considered. Furthermore, the quantitative aspect of the selective photothermolysis model

is not sufficient to calculate critical parameters such as the breakdown thresholds and cannot serve as a platform for quantitative comparison with the experimental results. The effect of adiabatic heating on the breakdown threshold in tissue has been quantitatively analyzed in terms of a photomechanical model based on the same photothermal mechanism [3]. In addition, a photochemical model was advanced to qualitatively interpret the corneal ablation in the deep UV region [4]. The above models assume strong or significant light absorption by the chromophores in selected spectral bands as the cause of tissue ablation without considering the possibility of laser-induced ionization or plasma. In contrast, a plasma model has been employed to explain the ocular tissue breakdown and ablation by nanosecond pulses in the visible and NIR regions in which plasma, induced by the strong electromagnetic fields of a short laser pulse without significant light absorption, is considered as the cause of breakdown [5]–[8]. The plasma ablation mechanism has been analyzed in detail using a rate-equation approach to obtain the dependence of the breakdown thresholds in water and transparent ocular tissues on various laser parameters [8]. It was found that the multiphoton absorption is most likely the pathway for generating seed electrons for the cascade ionization that is responsible for optical breakdown of transparent tissues at 532 and 1064 nm [7], [8]. However, the existing plasma model cannot be applied to the cases of nanosecond tissue ablation with significant light absorption because the role of tissue absorption in the ablation process remains unresolved.

The difficulties in understanding the tissue ablation or breakdown relate to both the complex nature of tissue optics and the strong-field regime of laser-induced breakdown. For tissue breakdown by nanosecond laser pulses, fundamental questions need to be answered: what is the mechanism of breakdown for the ablation of a strongly absorbing tissue and what is the relation between tissue absorption and the breakdown threshold? Visible or NIR nanosecond laser pulses have not been considered the first choices for tissue ablation in comparison to these pulses in the UV and mid-IR regions because of the relatively weak tissue absorption. However, a clear understanding of the ablation mechanism for tissue ablation with nanosecond pulses of wavelengths ranging from UV to NIR can provide insights on the laser-tissue interaction in the strong field regime and may lead to new methods of tissue or pigment breakdown inside the tissue for the relatively large penetration depth afforded in the visible and NIR regions.[9] Recently, experimental studies have been published on soft tissue ablation by nanosecond laser pulses at multiple wavelengths from 1064 to 213 nm [10], [11].

Manuscript received April 1, 2003; revised August 12, 2003.

Q. Fang is with the Department of Physics, East Carolina University, Greenville, NC 27858-4353 USA and also with the Biophotonics Research and Technology Development, Cedars-Sinai Medical Center, Los Angeles, CA 90048 USA.

X.-H. Hu is with the Department of Physics, East Carolina University, Greenville, NC 27858-4353 USA.

Digital Object Identifier 10.1109/JQE.2003.820837

In this report, we present a new plasma ablation model that can explain quantitatively the experimental results on the wavelength and spot-size dependence of the breakdown threshold and the ablation rate above the threshold at 1064 nm. The theoretical modeling will be presented in the next section, followed by the experimental results of breakdown probability measurements. We conclude with a discussion comparing the model predictions with the experimental results and application of this new plasma model to ablation of other types of soft tissues by nanosecond pulses.

II. MODELING

Human and porcine skin tissues have microscopically heterogeneous structures which are similar in their morphology, cellular composition, and physiological properties. The porcine skin is often used as a model of human skin [12]. The optical properties of the skin have been investigated from UV to NIR [13]–[17], and it has been shown that the light absorption in the skin becomes significant in the UV region which is electronic in origin and of broad-band resonance in nature. Based on the breakdown probability measurements, we have determined previously that the breakdown threshold of porcine skin epidermis in electric field \mathcal{E}_{th} ranges from 10^8 V/m for 14-ns pulses at 1064 nm to 10^7 V/m for 12-ns pulses at 213 nm [10]. For such strong electromagnetic fields by the nanosecond pulses, one has to consider the possibility of laser-induced ionization and consequent plasma formation in modeling of tissue ablation. For this purpose, we use a modified rate equation to describe the temporal evolution of quasifree electron density $\rho(t)$ in the tissue within an illuminated volume V of tissue [5]

$$\frac{\partial \rho}{\partial t} = \eta \rho + \left(\frac{\partial \rho}{\partial t} \right)_{mp} + \left(\frac{\partial \rho}{\partial t} \right)_{ch} - g\rho(t). \quad (1)$$

The first two terms on the right-hand side of (1) represent respectively the rates of cascade ionization, with a probability rate of $\eta > 0$, and multiphoton ionization that have been previously discussed in detail [7], [8]. The multiphoton term needs to be included only in cases where ionization requires simultaneous absorption of two or more photons. The third term is the ionization rate through light absorption by chromophores in the skin and is defined as the chromophore ionization rate here. The last term describes the loss of the quasi-free electrons via recombination, trapping, and diffusion and will be neglected in our calculations of breakdown thresholds for nanosecond pulses because of the relatively long lifetime and diffusion time of those electrons in comparison with the pulse duration τ around 10 ns [5].

The first-order differential equation of (1) with $g \ll \eta$ can be formally solved as follows with their spatial dependence concealed for simplicity:

$$\rho(t) = \left\{ \int_0^t \left[\left(\frac{\partial \rho}{\partial t'} \right)_{mp} + \left(\frac{\partial \rho}{\partial t'} \right)_{ch} \right] \times \exp \left(- \int_0^{t'} \eta dt'' \right) dt' \right\} \exp \left(\int_0^t \eta dt' \right) \quad (2)$$

where we assumed an initial condition that pre-existing quasi-free electron density is negligible at the start of the laser pulse $\rho(0) \approx 0$ and t is limited to τ so that the last term of (1) can be safely ignored. The rates of cascade and multiphoton ionization, $\eta\rho$ and $(\partial\rho/\partial t)_{mp}$, have been given in [8] and these results are used in this paper. We will derive the chromophore ionization rate, $(\partial\rho/\partial t)_{ch}$, below by first obtaining the quasi-free electron density due to the chromophore ionization $\rho_{ch}(t)$.

The major chromophores in the skin epidermis include melanosomes, whose absorption increases steeply as the light wavelength λ decreases to 300 nm or less, and proteins of urocanic acid, tryptophane and tyrosine, that all exhibit the first UV absorption peak for λ between 260 and 280 nm [13], [17]. To describe the chromophore ionization in the optical breakdown of the skin epidermis, it is necessary to make several assumptions regarding the optical, electronic, and thermal properties of the tissue and chromophores. We start by assuming that various major chromophores in the skin epidermis can be represented by a mean absorption cross section σ_a which is a function of wavelength and relates to the bulk absorption coefficient through

$$\mu_a = n_{ch}\sigma_a \quad (3)$$

where n_{ch} is the number density of the chromophores in the tissue. When a single chromophore is heated to a high temperature by the laser pulse, the electrons are freed from molecules due to thermal excitation. So we obtain the corresponding quasi-free electron density within V as

$$\rho_{ch} = n_{ch}N_bP \quad (4)$$

where N_b is the average number of bound electrons per chromophore available for ionization and P is the probability for a bound electron being thermally ionized. Both (3) and (4) are valid if the average distance between chromophores is much larger than their sizes. The thermal properties of the chromophores are assumed to be those of melanosome organelles [15] with specific heat $c_{ch} = 2.51 \times 10^3$ J/(kg·K), mass density $\rho_{ch} = 1.35 \times 10^3$ kg/m³, and a volume v_{ch} with an equivalent radius $R_{ch} \approx 1$ μ m. The number density of the chromophores in the skin tissues n_{ch} is given by $n_{ch} = f_{ch}/v_{ch}$, where f_{ch} is the volume ratio of the chromophore to skin. For melanosomes in the epidermis, f_{ch} varies with skin color, location, and age, and we adopt a value of n_{ch} as 1×10^{15} m⁻³ based on an estimated melanosome-to-skin volume ratio of 0.5% for light skin [16]. This corresponds to an average center-to-center distance of 10 μ m for chromophores, thus confirming the validity of (3) and (4). The ground substance of the skin epidermis between the chromophores is assumed to have properties close to those of water with specific heat $c_w = 4.19 \times 10^3$ J/(kg·K), mass density $\rho_w = 1.00 \times 10^3$ kg/m³, and thermal conductivity $\kappa_w = 0.57$ J/(m·s·K) with negligible absorption in the spectral region from 200 to 1300 nm. We should point out here that the use of optical and thermal properties of the melanosome for epidermis chromophores is mainly due to their availability in the literature. Since the melanosomes are only one type

of major chromophores in the epidermis from UV to NIR, it is therefore expected that the accuracy of our modeling can be significantly improved as the detailed knowledge on other epidermis and skin chromophores becomes available and the complexity of skin chromophore distribution can be taken fully into account.

A necessary condition for the chromophore ionization pathway to become important in generating quasi-free electrons lies in the adiabatic heating of the chromophores by nanosecond laser pulses. The speed of thermal energy transporting out of an illuminated chromophore can be estimated by considering the thermal diffusion over a distance of $2R_{\text{ch}}$ as

$$v_{\text{th}} = \frac{\kappa_{\text{ch}}}{2\rho_{\text{ch}}c_{\text{ch}}R_{\text{ch}}} \approx 0.1 \left(\frac{\text{m}}{\text{s}}\right) \quad (5)$$

where we assumed the thermal conductivity of the chromophore $\kappa_{\text{ch}} \approx \kappa_{\text{w}}$. The characteristic time of thermal conduction over $2R_{\text{ch}}$ is consequently about $20 \mu\text{s}$ and the adiabatic heating is achieved for a laser pulse of about 10 ns long. With similar arguments, one can show that the laser-induced pressure within a chromophore has a similar dissipation time and thus the changes in the chromophore volume can be neglected during a nanosecond pulse. This has been discussed in terms of inertial confinement [3].

Next we turn our attention to finding $\rho_{\text{ch}}(t)$ under the assumption that local thermal equilibrium is reached in a chromophore over the time scale of nanoseconds. Since the absorption peaks of major epidermis chromophores have been determined to be around 270 nm ($\sim 4.6 \text{ eV}$) [13], [17], we use a two-band model to describe the chromophore ionization in which the thermally excited quasi-free electrons occupy an energy band with lowest energy $E_{\text{ion}} = 4.60 \text{ eV}$ above a bound-state band populated by bound electrons. We further assume that the energy distribution of the electrons follows the energy-band model of amorphous semiconductors with the chemical potential μ located approximately in the middle of the gap between the two bands: $\mu \approx E_{\text{ion}}/2$. The density of the state for the electrons in the ionized states of upper band with energy $\varepsilon \geq E_{\text{ion}}$ may thus be written as [18]

$$g(\varepsilon) = 8\pi \left(\frac{2m_e}{h^2}\right)^{\frac{3}{2}} \sqrt{\varepsilon - E_{\text{ion}}}. \quad (6)$$

Hence, the density of quasi-free electrons with energy $\varepsilon \geq E_{\text{ion}}$ is obtained by

$$\begin{aligned} n(E_{\text{ion}}, T) &= \int_{E_{\text{ion}}}^{\infty} g(\varepsilon) f(\varepsilon, T) d\varepsilon \\ &= 8\pi \left(\frac{2m_e}{h^2}\right)^{\frac{3}{2}} \int_{E_{\text{ion}}}^{\infty} \frac{\sqrt{\varepsilon - E_{\text{ion}}} d\varepsilon}{e^{(\varepsilon - \mu)/k_B T} + 1} \end{aligned} \quad (7)$$

where the electrons follow the Fermi–Dirac distribution function $f(\varepsilon, T)$, m_e is the electron mass, h is the Plank constant, and k_B is the Boltzmann constant. For $T \leq 10^4 \text{ K}$, satisfied for all the calculations presented in this report, we find $e^{(E_{\text{ion}} - \mu)/k_B T} \gg 1$ for nondegenerate electron distributions.

Therefore, the function $f(\varepsilon, T)$ can be approximated by the Boltzmann distribution and (7) becomes

$$\begin{aligned} n(E_{\text{ion}}, T) &\approx 8\pi \left(\frac{2m_e}{h^2}\right)^{\frac{3}{2}} e^{\mu/k_B T} \int_{E_{\text{ion}}}^{\infty} e^{-\varepsilon/k_B T} \sqrt{\varepsilon - E_{\text{ion}}} d\varepsilon \\ &= 8\pi \left(\frac{2m_e}{h^2}\right)^{\frac{3}{2}} \frac{\sqrt{\pi}}{2} (k_B T)^{3/2} e^{(\mu - E_{\text{ion}})/k_B T}. \end{aligned} \quad (8)$$

Similarly, we can find the density of all electrons, n_{total} , which is nearly temperature-independent because the critical electron density for plasma formation ($\sim 10^{24} \text{ m}^{-3}$) is very small in comparison with the bound (valence) electron density ($\sim 10^{29} \text{ m}^{-3}$). Therefore,

$$\begin{aligned} n_{\text{total}}(T) &\approx n_{\text{total}}(0) = \int_0^{\infty} g(\varepsilon) f(\varepsilon, 0) d\varepsilon \\ &= 8\pi \left(\frac{2m_e}{h^2}\right)^{\frac{3}{2}} \frac{2}{3} \mu^{3/2} \end{aligned} \quad (9)$$

where we neglected the temperature dependence of μ . With these results, we obtain the thermal ionization probability for a bound electron within a skin chromophore at temperature T as

$$\begin{aligned} P &= \frac{n(E_{\text{ion}}, T)}{n_{\text{total}}(T)} \\ &\approx \frac{3\sqrt{\pi}}{4} \left(\frac{k_B T}{E_{\text{ion}}/2}\right)^{\frac{3}{2}} e^{-E_{\text{ion}}/2k_B T} \end{aligned} \quad (10)$$

with μ replaced by $E_{\text{ion}}/2$ in the last step. For a single nanosecond laser pulse starting at $t = 0$, the energy deposited into a chromophore is determined by the laser fluence $F(t)$ given by the time integral of the irradiance $I(t)$, $F(t) = \int_0^t I(t) dt$. Neglecting the temperature dependence of c_{ch} and ρ_{ch} , justified under the condition of inertial confinement, the local temperature within an illuminated chromophore can be found to be

$$\begin{aligned} T &= T_0 + \frac{F(t)\sigma_a}{c_{\text{ch}}v_{\text{ch}}\rho_{\text{ch}}} \\ &= T_0 + \frac{F(t)\mu_a}{c_{\text{ch}}\rho_{\text{ch}}f_{\text{ch}}} \end{aligned} \quad (11)$$

where $T_0 = 300 \text{ K}$ is the ambient temperature. Combining, we find

$$\begin{aligned} \rho_{\text{ch}}(t) &= \frac{3\sqrt{\pi}n_{\text{ch}}N_b}{4} \left[\frac{2k_B}{E_{\text{ion}}} \left(T_0 + \frac{F(t)\mu_a}{c_{\text{ch}}\rho_{\text{ch}}f_{\text{ch}}} \right) \right]^{\frac{3}{2}} \\ &\quad \times \exp \left\{ -\frac{E_{\text{ion}}}{2k_B \left(T_0 + \frac{F(t)\mu_a}{c_{\text{ch}}\rho_{\text{ch}}f_{\text{ch}}} \right)} \right\}. \end{aligned} \quad (12)$$

One can observe that the wavelength dependence of the laser-induced chromophore ionization originates from that of the tissue absorption coefficient μ_a .

To calculate the total quasi-free electron density $\rho(t)$ from (2), one needs also the rates of cascade and multiphoton ioniza-

TABLE I
OPTICAL PARAMETERS OF SKIN EPIDERMIS AND BREAKDOWN THRESHOLDS

| λ (nm) | 1064 | 532 | 266 | 213 |
|---|------------------------|------------------------|------------------------|------------------------|
| $\pi w_{x0} w_{y0}$ (m ²) | 1.98×10^{-10} | 4.91×10^{-10} | 3.14×10^{-10} | 3.14×10^{-10} |
| μ_a (m ⁻¹) ⁽¹⁾ | 4.2×10^3 | 4.0×10^3 | 1.0×10^5 | 5.0×10^5 |
| μ'_s (m ⁻¹) ⁽¹⁾ | 2.3×10^3 | 1.2×10^4 | 6.3×10^4 | 9.5×10^4 |
| V (m ³) | 2.2×10^{-14} | 3.5×10^{-14} | 1.4×10^{-15} | 3.5×10^{-16} |
| $(I_{th})_{exp}$ (W/m ²) ⁽²⁾ | 2.72×10^{13} | 1.17×10^{13} | 3.03×10^{12} | 6.27×10^{11} |
| $dY/d(\log I)$ ⁽²⁾ | 4.81 | 7.94 | 5.54 | 7.29 |
| $(I_{th})_{cal}$ (W/m ²) | 1.57×10^{12} | 1.08×10^{12} | 1.15×10^{11} | 2.33×10^{10} |
| $(I_{th})_{exp} / (I_{th})_{cal}$ | 17 | 11 | 26 | 27 |

(1) The absorption and reduced scattering coefficients of the skin epidermis are estimated from the compiled data in [14] and their extrapolation to 1064 and 213nm.

(2) The thresholds at 10% ablation probability and the slope of linear regression lines were obtained by averaging over the two sets of data shown in Fig. 4.

tion which have been discussed in detail for optical breakdown in water by nanosecond pulses without chromophores [8]. We adopt the same expressions for the two rates and same values of parameters used in [8] except that E_{ion} is replaced by 4.60 eV since we consider the two ionization pathways only inside the chromophores within the illuminated volume V . The contributions to $\rho(t)$ from the bound electrons in water-like ground substance to the multiphoton ionization is negligible since the corresponding value of E_{ion} ($=6.5$ eV) for water is significantly larger than that of the chromophore. By taking a partial derivative of $\rho_{ch}(t)$ with respect to time, we are now in a position to numerically calculate $\rho(t)$ given the laser fluence $F(t)$ and tissue optical parameters. For simplicity, we consider a square laser pulse with a temporal profile given by $F(t) = I_0 t$ for $0 < t < \tau$ and $F(t) = 0$ otherwise. To compare with our earlier experimental results (see Table I of [10]), we adopt the following parameters: laser beam spot area $= \pi w_{x0} w_{y0}$, penetration depth $D = [3\mu_a(\mu_a + \mu'_s)]^{-1/2}$ with μ'_s as the reduced scattering coefficient of the skin tissue [14], $V = \pi w_{x0} w_{y0} D$, $n_{ch} \approx 1.0 \times 10^{15}$ m⁻³, $m_{ch} \approx 2 \times 10^{-16}$ kg, and $N_b \approx 1.0 \times 10^{11}$. Values of other parameters are listed in Table I with footnotes on the source of data. We note here that the illuminated volume V represents only the minimal value of the volume relevant to the consideration of breakdown at the breakdown threshold. As the laser irradiance I increases, the relevant volume in which the irradiance value exceeding the breakdown threshold will become larger than V . Furthermore, the calculation of the penetration depth D is based on the light diffusion model [19], which may not be very accurate when applied to the tissue surface.

To illustrate the effect of different pathways on ionization at the four wavelengths, we determine the dependence of quasi-free electron density $\rho_i(t)$ on laser irradiance I at $t = \tau/2$ for a selected ionization pathway i ($=ca$ for cascade, mp for multiphoton, ch for chromophore) by setting the other two of three rates, η , $(\partial\rho/\partial t)_{mp}$ and $(\partial\rho/\partial t)_{ch}$, to zero in (2). In addition, the full solution of the rate equation, $\rho(t)$ in (2), is numerically obtained and shown in Fig. 1 together with $\rho_i(t)$ at $t = \tau/2$. The reasons of calculating the quasi-free electron densities at the mid-point of pulse duration lie in the fact that both cascade and multiphoton ionization depend only on laser

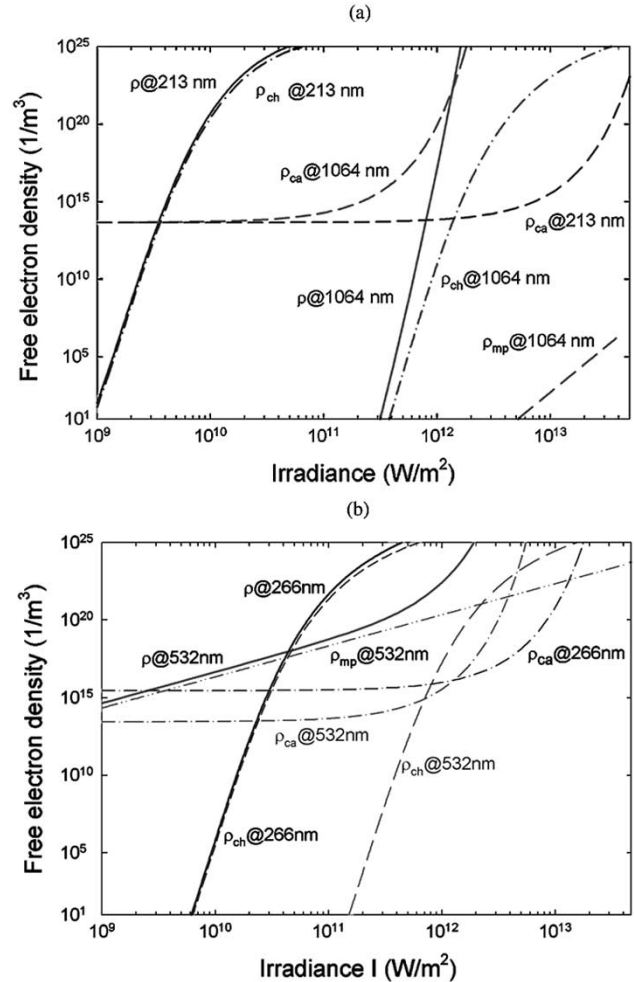


Fig. 1. Dependence of the quasi-free electron densities at the mid-point of pulse duration ($\tau/2$) on peak laser irradiance for each of three ionization pathways and the total quasi-free electron density represented by the thick solid lines at the wavelengths of (a) 1064 and 213 nm and (b) 532 and 266 nm.

irradiance I which reaches the maximum value I_{max} at $\tau/2$ for pulses of symmetric temporal shape. For the wavelengths of 213 and 266 nm, the multiphoton pathway is not included since the ionization energy E_{ion} is less than the single photon

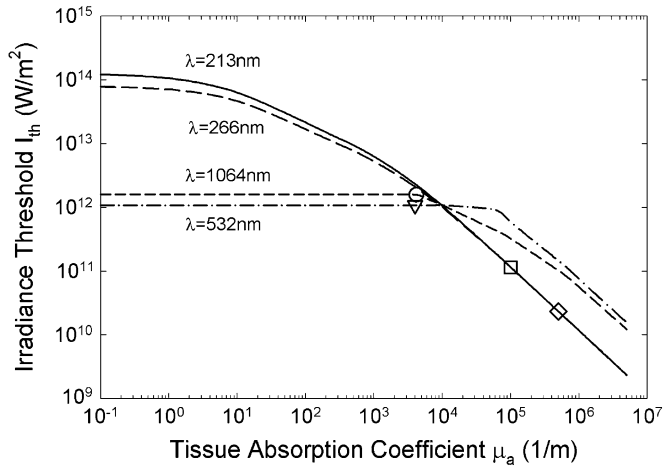


Fig. 2. Dependence of the breakdown thresholds on tissue absorption coefficient at four values of wavelength λ . The measured breakdown thresholds at 10% probability are marked with the symbols (see also Table I) corresponding to $\lambda = 1064$ nm (\circ), 532 nm (∇), 266 nm (\square), and 213 nm (\diamond).

energy. At 1064 nm, only the chromophore and multiphoton ionization processes can generate the seed electrons, but the latter is much weaker than the former since $\rho_{\text{mp}} \propto I^4$. Once the seed electrons exist in the illuminated volume of the laser beam, the cascade ionization pathway dominates the ionization, leading to the breakdown of the tissue due to strong field by the nanosecond pulses. Therefore, the chromophore and cascade ionization pathways are the primary factors in determining the breakdown threshold of the skin tissues by NIR nanosecond pulses. The strong absorption of the nanosecond pulses at 213 and 266 nm by the chromophores dominates the ionization process, shown in Fig. 1(a) and (b), respectively, while the cascade pathway does not play a significant role because of the relative weak field by the laser pulse for $I_{\text{max}} < 10^{12}$ W/m². In contrast, the multiphoton ionization pathway provides the seed electrons at 532 nm for the cascade ionization to start and control the ionization process because the chromophore absorption is very weak. From the results shown in Fig. 1, we conclude that our plasma ablation model is capable of explaining the optical breakdown of the skin tissues in terms of chromophore ionization when optical absorption is strong. This model thus provides a theoretical platform to quantitatively understand the probabilistic behavior of the ablation process near the breakdown threshold observed at the four wavelengths [10].

The breakdown threshold in laser irradiance can be determined from this new model by defining a critical value for the total quasi-free electron density, $\rho(\tau/2) = \rho_{\text{th}} = 10^{24}$ m⁻³, at which the breakdown or tissue ablation is assumed to occur as a result of plasma formation [5]. The effects of the three ionization pathways on the breakdown of biological tissues can be seen from a different perspective in Fig. 2 where the irradiance thresholds I_{th} are plotted as a function of tissue absorption coefficient μ_a at the four wavelengths. These results were calculated by assuming μ_a as a variable independent of wavelength to account for multiple types of tissues in different applications. For the regime of weak absorption with $\mu_a < 10^4$ m⁻¹, the multiphoton ionization plays the primary role in determining

the breakdown threshold since it is the only pathway to generate the seed electrons for cascade ionization to start. In comparison, the chromophore ionization dominates over both the cascade and multiphoton ionization pathways for the strong absorption regime with $\mu_a > 10^5$ m⁻¹. Under this condition, the breakdown thresholds become nearly wavelength-independent because the chromophore absorption is the only factor in determining the breakdown threshold. To compare with the measured values of breakdown threshold in the skin epidermis, I_{th} , at 10% ablation probability [10], we show the data with the square symbols in Fig. 2 and list the calculated thresholds and the ratios of measured thresholds to the calculated values at the four wavelengths in Table I. We note that no attempts have been made to adjust the parameter values, such as E_{ion} , f_{ch} , and R_{ch} , to fit the calculated results to the measured results since our effort is focused on the wavelength dependence. As shown in Table I, the experimental values for irradiance threshold are larger than the calculated values by a factor between 8 to 23 and the agreement of wavelength dependence of the two sets of threshold values is relatively good, given the large uncertainty in the optical parameters of the skin epidermis.

III. EXPERIMENTAL RESULTS

A major issue in the quantitative study of tissue ablation lies in the accurate determination of the breakdown threshold. In a previous report, we reported the identification of an optical signature of the breakdown in fresh porcine skin tissue samples [10]. The spectral line of Na atoms at 589 nm from the secondary radiation has been verified to provide a reliable signal in real time that is coincident with the occurrence of ablation in the skin tissue. The experimental method to measure the breakdown thresholds and determine their wavelength dependence has been described in detail previously [10]. Here we briefly summarize the experimental setup. A Q -switched Nd:YAG laser (Surlite I, Continuum) was used to generate pulses of 14 ns in full-width at half-maximum (FWHM) duration at a wavelength of 1064 nm. The second, fourth, and fifth harmonics of the fundamental pulses were generated with up to three nonlinear optical crystals and pulse durations were measured to be 12 ns. The laser beam was collimated before entering the nonlinear crystals and the fundamental and each harmonic were separated using either dichromatic mirrors or a UV prism. The selected laser beam was focused with a spherical lens of different focal length to vary the size of the beam at the waist. We measured the profile of each beam after the focusing lens at different distance from the waist along the optical axis (z axis) using a CCD camera based profilometer and determined its radii of the focal spot and M^2 factor from z dependence of the beam radii on the x and y axes [10]. A typical example is shown in Fig. 3 for determining the values of M^2 and the radii of the waist for a plano-convex spherical lens of focal length $f = 75$ mm. The values of M^2 were found to range between 1.2 and 1.4 for laser beams at the four wavelengths and focused with different lenses and diameters of the focal spot were further verified with a knife-edge method.

Fresh porcine skin samples have been used to measure the breakdown probability near the threshold within 30 h of animal euthanasia, and the procedures of sample preparation have been

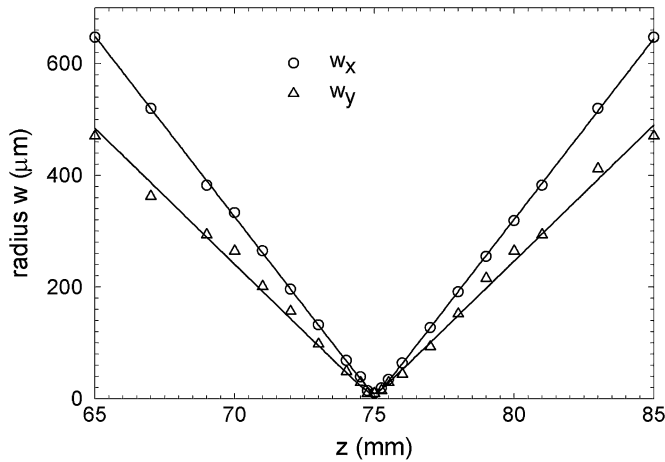


Fig. 3. Radii of the laser beam with $\lambda = 1064$ nm after a focusing lenses of 75-mm focal length as a function of distance on the z axis measured using a CCD camera-based laser beam profilometer. The solid lines are the fitting curves to obtain the radii of the waist w_{x0} and w_{y0} and M^2 along the x and y axes.

described previously [10]. The occurrence of breakdown was determined based on the presence of the spectral line at 589 nm in the secondary radiation from the ablated sample. The breakdown probability P near threshold was determined as the portion of 100 pulses incident on the sample with the occurrence of breakdown and the pulse energy was varied to measure P as a function of laser irradiance I at the specified wavelength and spot size. The skin sample, with the epidermis facing the incident laser beam, was translated during the experiment so that each pulse was incident on a fresh spot to ensure a single-pulse condition. Each set of breakdown probability data shown in Figs. 4 and 5 has been measured on the same skin tissue sample but different sets of data were obtained from different porcine skin samples and different pigs. To test if a set of percentage breakdown probability data, $P(I)$, follows a normal distribution with respect to $\log(I)$, we used the probit analysis in which the probit Y is related to percentage probability P as [20]

$$P = \frac{1}{\sqrt{2\pi}} \int_{-\infty}^Y \exp\left\{-\frac{1}{2}u^2\right\} du, \quad (13)$$

A log-normal distribution of $P(I)$ data is represented by the distribution of data along a straight line in a Y -versus- $\log(I)$ plot. The linear regression line of the data can be used to accurately determine the breakdown thresholds at specific value of probability and its slope, $dY/d(\log I)$, has been employed to examine the mechanism of ablation [21].

In Fig. 4, we show with filled symbols the probit of breakdown probability as a function of laser irradiance with focusing lens of $f = 75$ mm at 1064, 532, 266, and 213 nm. These results are consistent with our earlier data [10] represented by the unfilled symbols. In Table I, we list the mean value of the slope of the linear regression to the probit plots for the filled symbols and the mean breakdown thresholds at 10% of breakdown probability averaged over the two sets of data at each wavelength. To study the spot-size dependence of the breakdown threshold,

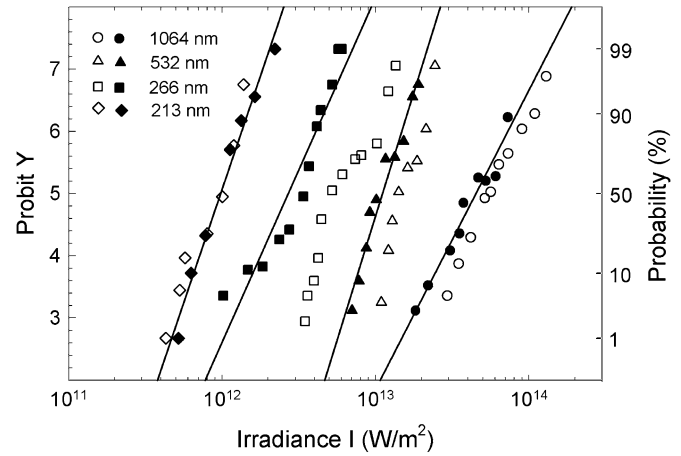


Fig. 4. Probit of ablation probability as a function of laser irradiance at the four wavelengths with the spot areas given in Table I. Solid lines are linear regression for each set of data represented by filled symbols and follow $Y = \alpha + \beta \log(I)$ with the slope β obtained as 4.81 (1064 nm), 7.94 (532 nm), 5.54 (266 nm), and 7.29 (213 nm). For comparison, other sets of data, which have been published in [10, Fig. 3(a)], are plotted by unfilled symbols for corresponding wavelengths and same spot radii. The values of percentage probability can be read off from the right vertical axis.

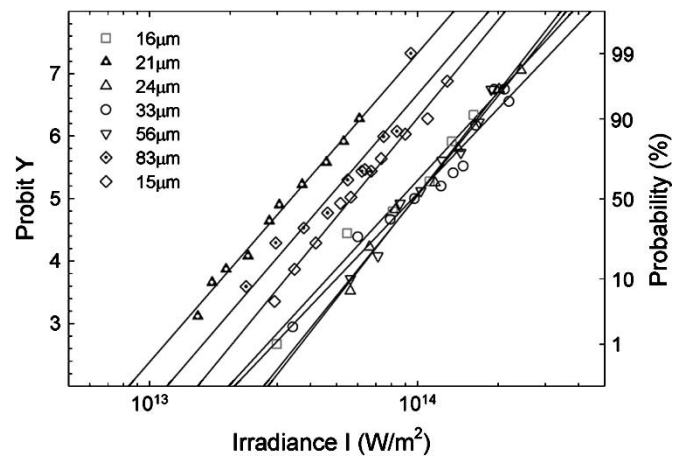


Fig. 5. Probit Y of ablation probability as a function of laser irradiance I at the wavelength of 1064 nm with different mean spot radii. Solid lines are linear regression for each set of data with the values of the slope factor β listed in Table II.

we carried out measurements of breakdown probability with different focusing lenses of various focal lengths at the wavelength of 1064 nm. With the tissue sample's surface located at the focal plane, the mean diameters of the focal spot varies between 15 and 83 μm as the focusing lens was changed with f ranging from 75 to 700 mm. The breakdown probability, in terms of the probit Y and measured at seven different spot sizes, are presented in Fig. 5 as a function of laser irradiance I . The slopes of the linear regression lines and the breakdown thresholds I_{th} at the probabilities of 10% were determined for each set of data and are listed in Table II together with the focal lengths of the focusing lenses and the resultant mean diameters of the illuminating spots. The results shown in Fig. 5 exhibit no clear dependence of the breakdown probability on spot size. In comparison to the data of wavelength dependence shown in Fig. 4, the difference between the sets of data of different spot sizes is small and may be attributed to the variations in optical properties of

TABLE II
FOCAL SPOT DIAMETERS AND BREAKDOWN THRESHOLDS AT THE WAVELENGTH OF 1064 nm

| Focal length (mm). | 75 | 125 | 175 | 200 | 300 | 500 | 700 |
|---|------|------|------|------|------|------|------|
| Mean diameter (μm) | 15 | 16 | 21 | 24 | 33 | 56 | 83 |
| $(I_{\text{th}})_{\text{exp}} (\times 10^{13} \text{W/m}^2)^{(1)}$ | 2.72 | 4.68 | 1.86 | 5.50 | 5.01 | 5.62 | 2.57 |
| $(\mathcal{E}_{\text{th}})_{\text{exp}} (\times 10^7 \text{V/m})^{(1)}$ | 9.18 | 10.9 | 7.11 | 12.1 | 11.6 | 12.1 | 8.04 |
| $dY/d(\log I)$ | 5.23 | 4.67 | 4.94 | 5.31 | 4.50 | 5.48 | 4.99 |

(1) The threshold data were determined from the ablation of fresh porcine skin epidermis at 10% ablation probability.

the porcine skin samples since different porcine skin samples from different pigs were used.

IV. DISCUSSION

Ablation of soft tissues by laser pulses has attracted significant research attention over the last two decades. Among the observed phenomena associated with tissue ablation by nanosecond laser pulses, the presence of a breakdown threshold and its variation as a function of laser parameters and tissue optical properties are of fundamental importance to the understanding of the ablation mechanism. The plasma ablation model has been successfully used to explain the nature of the breakdown process by nanosecond laser pulses in transparent media such as the ocular tissues and water [22]. Because the existing plasma model does not consider tissue absorption, however, the interpretation of the tissue ablation has relied upon the photothermal or photochemical models in the cases of turbid tissues with strong absorption such as the skin tissues in the UV and visible regions. None of the photothermal and photochemical models, however, considers the possibility of ionization due to the light absorption by chromophores. The necessity of including chromophores ionization in the modeling of tissue ablation by nanosecond pulses is manifested from the very large rise in the local temperature within a chromophore that can be estimated from (11). Using the values of calculated irradiance thresholds and other parameters listed in Table I, one finds that the magnitude of $T - T_0$ is between 10^3 to 10^4 K from UV to NIR, much higher than the vaporization temperature of water under ambient pressure and thus the possibility of ionization must be taken into account. The new plasma ablation model introduced in this report incorporates the chromophore ionization pathway into the approach of the rate equation to consider the role of tissue absorption in the ionization process leading to tissue breakdown and ablation. Numerical solutions of the rate (1), taking into account all three ionization pathways, show that the chromophore ionization plays a significant role in the skin tissue ablation in both the UV and NIR regions. It dominates the quasi-free electron generation in the UV region in which the tissue absorption is strong and provides the seed electrons in the NIR region for starting the cascade ionization. In the visible region where two-photon absorption can lead to the generation of seed electrons, multiphoton ionization instead provides the seeds for cascade ionization to form plasma and ablate the tissue. With this new model, we were able to show that the breakdown thresholds, defined at the irradiances causing the critical density of quasi-free electrons [5], monotonically decrease from NIR to UV, as shown in Fig. 2

and Table I. Even though the calculated thresholds still differ significantly from the measured values, smaller by factors ranging from 11 to 27, the relatively good agreement between the wavelength dependences of the thresholds provides us the confidence that this new plasma model should yield a much better platform for future study of the tissue ablation mechanism than the existing models. Furthermore, the accuracy of the calculations based on our new plasma model is expected to improve when accurate knowledge of the chromophores distribution and optical properties of the tissues affecting light distribution become available.

The weak and fluctuating dependence of the breakdown threshold on the spot size at the wavelength of 1064 nm, shown in Fig. 5 and Table II, appears puzzling in comparison to that in transparent and homogeneous solids. It has been reported that the threshold field \mathcal{E}_{th} of optical breakdown by picosecond and nanosecond pulses at the wavelength of 1064 nm depends on the illuminated volume V at the focal spot and pulse duration τ through $\mathcal{E}_{\text{th}} = (A/\tau^{1/4}V) + C$ where A and C are material constants [23]. For the turbid medium of skin considered in our model, V at the same wavelength is determined by the area of the focal spot since the penetration depth based on the light diffusion model remains the same. Thus, one would expect the field threshold for breakdown to decrease with increasing diameter, which is clearly not the case for the data listed in Table II. This behavior can be well explained by our new plasma model in which the skin tissue is treated as an inhomogeneous material with uniformly distributed chromophores of sizes near $1 \mu\text{m}$ in a water-like host medium. Note that the value of the chromophore density adopted in our model, $n_{\text{ch}} \approx 1.0 \times 10^{15} \text{m}^{-3}$, corresponds to about 20 chromophores even in the smallest V at 1064 nm (see Table II), and the optical breakdown starts within the chromophores because of their smaller ionization energy than the host medium. Therefore, it is expected that the optical breakdown in the skin tissue occurs locally within chromophores and should be independent of the spot size for nanosecond pulses at the same wavelength. Additionally, the similar values of $dY/d(\log I)$ between different sets of data in Fig. 5 show that the probit analysis can be used as a tool insensitive to the sample variations to allow study of underlying mechanism of the tissue ablation.

The probabilistic behavior of the optical breakdown process near threshold has been considered as the intrinsic nature of the cascade or impact ionization in which the quasi-free electrons are accelerated in the oscillating electric field of the laser pulse either ballistically or through elastic collisions [5], [21]. The latter form of electron acceleration would yield a parabolic relation between the logarithm of breakdown probability P and the

reciprocal of the electric field \mathcal{E} , i.e., $P = P_0 \exp(-K^2/\mathcal{E}^2)$ where K is a fitting parameter [24]. This relation between P and \mathcal{E} is observed in all sets of our data presented in Fig. 4 and 5 (not shown) and has been previously discussed in terms of electron scattering during cascade ionization [10]. At the wavelengths of 1064 and 532 nm, this is consistent with the current model since the breakdown is dominated by cascade ionization once the seed electrons are generated by either chromophore or multiphoton ionization processes. In the UV region of strong tissue absorption, however, the breakdown is fully dominated by the chromophores' ionization according to our model and is shown in Fig. 1. Therefore, the probabilistic nature of the breakdown process at 266 and 213 nm should be caused by the distribution of chromophores instead of by the microscopic collisions experienced by the free electrons. This hypothesis is supported by the fact that the illuminated volume V is significantly reduced at the UV wavelengths for the large tissue absorption coefficient μ_a . Using the values of V in Table I and the chromophore density n_{ch} , one can immediately see that the number of chromophores in V is on the order of 1 for the wavelengths of 266 and 213 nm. Although both the radius of the focal spot and the penetration depth D remain as constants as the pulse energy increases because they are defined relative to the peak irradiance at the center of beam on the sample surface, the illuminated volume with irradiance above the breakdown threshold of chromophores will become larger than V . Thus, the breakdown probability should increase with the pulse energy because of the increasing probability of chromophores being illuminated above the breakdown threshold. In comparison with the data in visible and NIR regions due to the electron collisions in cascade ionization, the probabilistic behavior of breakdown in the deep UV regions demonstrates an extrinsic nature of the breakdown mechanism. Based on this hypothesis, we expect steep slopes of the probability data, $dY/d(\log I)$, at UV wavelengths because the range of laser irradiances between $P = 0$ and $P = 100\%$ is anticipated to be narrow. This is certainly the case for the data at 213 nm as shown in Fig. 4 but not quite so for the data at 266 nm, which may be attributed to the stronger electric field of laser pulse at breakdown threshold than that at 213 nm and possible contribution to the free electron generation by the cascade process. One way to test the validity of this hypothesis is to measure the spot-size dependence of the breakdown probability at the UV wavelengths. We have not been able to accomplish the test due to the energy limitation of nanosecond pulses at 266 and 213 nm obtained through harmonic generation. We hope the test can be carried out in the near future.

In summary, we have introduced a new plasma model to explain the skin tissue ablation with nanosecond laser pulses from UV to NIR by incorporating a new ionization pathway through light absorption by chromophores. By solving numerically a modified rate equation, we have shown that the new model can be used to calculate the breakdown thresholds as a function of laser and tissue parameters by nanosecond laser pulses in a broad spectrum from UV to NIR. Good agreements have been found between the predicated and measured results on the wavelength and spot size dependence of the breakdown threshold without adjustable parameters. Furthermore, the new model is capable of providing insights on the probabilistic behavior of

the breakdown process near the threshold. The new model introduced in this report presents a platform to understand clearly the fundamental mechanisms underlying the complex tissue ablation process and to simulate numerically the ablation process of biological tissues by nanosecond laser pulses with the laser and tissue parameters. It should be pointed out that much remains to be refined for the new plasma model. We believe that the accuracy of the new model can be significantly improved and its utility can be extended to other soft tissues once an accurate spectral database on the bulk optical properties of soft tissues becomes available. Furthermore, this model may be applied to soft tissue ablation by nanosecond pulses in infrared regions beyond the wavelength of 1200 nm, such as the mid-infrared region between 2 and 5 μm , by taking into account the strong absorption and ionization process in the host medium.

REFERENCES

- [1] R. R. Anderson and J. A. Parrish, "Selective photothermolysis: Precise microsurgery by selective absorption of pulsed radiation," *Science*, vol. 220, pp. 524–527, 1983.
- [2] M. Beatrice, T. Alora, and R. R. Anderson, "Recent developments in cutaneous lasers," *Lasers Surg. Med.*, vol. 26, pp. 108–118, 2000.
- [3] I. Itzkan, D. Albagli, M. L. Dark, L. T. Perelman, C. von Rosenberg, and M. S. Feld, "The thermoelastic basis of short pulsed laser ablation of biological tissue," in *Proc. Nat. Acad. Sci. USA*, vol. 92, 1995, pp. 960–1964.
- [4] R. Srinivasan, "Ablation of polymers and biological tissue by ultraviolet lasers," *Science*, vol. 234, pp. 559–565, 1986.
- [5] N. Bloembergen, "Laser-induced electric breakdown in solid," *IEEE J. Quantum Electron.*, vol. QE-10, pp. 375–386, 1974.
- [6] S. L. Trokel, "Optical breakdown and YAG laser physics," in *YAG Laser Ophthalmic Microsurgery*, S. L. Trokel, Ed. Norwalk, CT: Appleton-Century-Crofts, 1983, ch. 2.
- [7] A. Vogel, S. Busch, K. Jungnickel, and R. Birngruber, "Mechanisms of intraocular photodisruption with picosecond and nanosecond laser pulses," *Lasers Surg. Med.*, vol. 15, pp. 32–43, 1994.
- [8] P. K. Kennedy, "A first-order model for computation of laser-induced breakdown thresholds in ocular and aqueous media: Part I: Theory," *IEEE J. Quantum Electron.*, vol. 31, pp. 2241–2249, 1995.
- [9] X. H. Hu, W. A. Wooden, S. J. Vore, M. Cariveau, Q. Fang, and G. W. Kalmus, "In vivo study of intradermal focusing for tattoo removal," *Lasers Medical Sci.*, vol. 17, pp. 154–164, 2002.
- [10] X. H. Hu, Q. Y. Fang, M. J. Cariveau, X. N. Pan, and G. W. Kalmus, "Mechanism study of porcine skin ablation by nanosecond laser pulses at 1064, 532, 266 and 213 nm," *IEEE J. Quantum Electron.*, vol. 37, pp. 322–328, 2001.
- [11] S. Sato, M. Ogura, M. Ishihara, S. Kawachi, T. Arai, T. Matsui, A. Kurita, M. Obara, M. Kikuchi, and H. Ashida, "Nanosecond, high-intensity pulsed laser ablation of myocardium tissue at the ultraviolet, visible, and near-infrared wavelengths: In-vitro study," *Lasers Surg. Med.*, vol. 29, pp. 464–473, 2001.
- [12] R. M. Lavker, G. Dong, P. S. Zheng, and G. F. Murphy, "Hairless micropig skin," *Am. J. Pathol.*, vol. 138, pp. 687–697, 1991.
- [13] R. R. Anderson and J. A. Parrish, "The optics of human skin," *J. Invest. Dermatol.*, vol. 77, pp. 13–19, 1981.
- [14] M. J. C. van Gemert, S. L. Jacques, H. J. C. M. Sterenborg, and W. M. Star, "Skin optics," *IEEE Trans. Biomed. Eng.*, vol. 36, pp. 1146–1154, 1989.
- [15] S. L. Jacques and D. J. McAuliffe, "The melanosomes: Threshold temperature for explosive vaporization and internal absorption coefficient during pulsed laser irradiation," *Photochem. Photobiol.*, vol. 53, pp. 769–755, 1991.
- [16] K. Jimbow, W. C. Quevedo Jr., T. B. Fitzpatrick, and G. Szabo *et al.*, "Biology of melanocytes," in *Dermatology in General Medicine*, 4th ed, T. B. Fitzpatrick *et al.*, Eds. New York: McGraw-Hill, 1993, vol. 1, ch. 18.
- [17] A. R. Young, "Chromophores in human skin," *Phys. Med. Biol.*, vol. 42, pp. 789–908, 1997.
- [18] J. I. Pankove, *Optical Processes in Semiconductors*. Englewood Cliffs, NJ: Prentice-Hall, 1971, ch. 1.

- [19] A. Ishimaru, *Wave Propagation and Scattering in Random Media*. New York: Academic, 1978, vol. 1, ch. 9.
- [20] D. J. Finney, *Probit Analysis*, 3rd ed. Cambridge, U.K.: Cambridge Univ. Press, 1971, ch. 3. Table I.
- [21] D. Sliney and M. Wolbarsht, *Safety with Lasers and Other Optical Sources*. New York: Plenum, 1980, ch. 7.
- [22] C. A. Sacchi, "Laser induced electric breakdown in water," *J. Opt. Soc. Amer. B*, vol. 8, pp. 337–345, 1990.
- [23] E. W. Van Stryland, M. J. Soileau, A. L. Smirl, and W. E. Williams, "Pulse-width and focal-volume dependence of laser-induced breakdown," *Phys. Rev. B*, vol. 23, pp. 2144–2151, 1981.
- [24] B. K. Ridley, "Lucky-drift mechanism for impact ionization in semiconductors," *J. Phys. C*, vol. 16, pp. 3373–3388, 1983.



Qiyin Fang received the B.S. degree in physics from Nankai University, Tianjin, China, in 1995 and the M.S. degree in applied physics and the Ph.D. degree in biomedical physics from East Carolina University, Greenville, NC, in 1998 and 2002, respectively.

He is currently a Research Scientist in the Cedar-Sinar Medical Center, Los Angeles, CA. His research interests are in the laser-tissue interaction and optical diagnosis with time-resolved fluorescence methods.



Xin-Hua Hu received the B.S. and M.S. degrees in physics from Nankai University, Tianjin, China, in 1982 and 1985, respectively, the M.S. degree in physics from Indiana University at Bloomington in 1986, and the Ph.D. degree in physics from University of California, Irvine, in 1991.

In 1995, he joined the physics faculty at East Carolina University, Greenville, NC, and established the Biomedical Laser Laboratory (<http://bm-laser.physics.ecu.edu>). He is currently directing research in soft tissue ablation by nanosecond laser pulses, tissue optics and spectroscopy, light scattering by biological cells, medical imaging for diagnosis and monitoring treatment of cancers, and Monte Carlo and other large-scale parallel computation of light distribution in turbid systems.